Optimization of hydrocalumite preparation under microwave irradiation for recovering aluminium from a saline slag

Alejandro Jiménez [a], Alexander Misol [a], Álvaro Morato [a], Vicente Rives [a,*], Miguel A. Vicente [a], Antonio Gil [b]

[a] GIR–QUESCAT, Departamento de Química Inorgánica, Universidad de Salamanca, E–37008 Salamanca, Spain
[b] INAMAT²–Departamento de Ciencias, Universidad Pública de Navarra, E–31006 Pamplona, Spain

ARTICLE INFO

ABSTRACT

Aluminium was successfully extracted by treating an aluminium slag with aqueous NaOH under reflux conditions. This solution was purified by precipitation of silicon species by addition of HCl up to pH = 1, and used for preparing hydrocalumite ($Ca_2Al(OH)_6Cl \cdot 2H_2O$) by the coprecipitation method. The effect of temperature on the properties of hydrocalumite prepared under microwave (MW) irradiation was studied. Characterization of the obtained solid was carried out by powder X-ray diffraction (PXRD), thermal analysis, FT–IR spectroscopy, chemical analysis, electron microscopy and N_2 adsorption–desorption at −196 °C. The results showed that the use of the extracted aluminium solution allowed to obtain hydrocalumite by the coprecipitation method and that the temperature of the MW ageing treatment had a large effect on the formation of side phases, in addition to hydrocalumite. The results here reported demonstrate that formation of hydrocalumite is an effective method for the recovering of aluminium from its waste.

1. Introduction

According to the World Bureau of Metal Statistics, consumption of aluminium was 62.8 million metric tons in 2019 (World Bureau of Metal Statistics, 2020), with an increase of 55% in a period of only nine years (40.6 million metric tons in 2010 (Fig. 1). This increase in its use is mainly due to the excellent properties of this metal, its low density (2.70 g/cm³), low melting point (660 °C) and corrosion resistance, among other properties, allow its use in a large variety of applications (Sverdlin, 2003).

Industrial aluminium production is carried out by combination of the Bayer and Hall–Héroult processes (*primary* aluminium production) (Gil, 2005). The requirement of electric energy is high and various wastes, such a *red mud*, are generated, with a potentially enormous danger on the environment (Gil, 2005). Fortunately, aluminium can be recycled and reused maintaining its properties. In this way, *secondary* aluminium production is based on recycling of the metal. This second process requires less energy than primary aluminium production. Unfortunately, an important waste is generated during this process, the so called *Salt Cake or Saline Slag* (Gil, 2005; Bruckard and Woodcock, 2007, 2009), generated from the use of flux salts (mainly NaCl and KCl) to melt

aluminium scraps. As the European Union considers this residue as a hazardous waste (Directive 2010/75/EU, 2010), various procedures for managing it have been proposed (Gil, 2005; Gil and Korili, 2010, 2016; Tsakiridis, 2012; Tsakiridis et al., 2013; Gil et al., 2014, 2018a, 2018b). Thus, Gil and Korili (2010, 2016) have studied the current situation of managing the wastes, concluding that the best option is to recover metallic aluminium and to dispose the non–metallic fraction in controlled landfills. Gil and co–workers have also used saline slags as an adsorbent (Gil et al., 2014, 2018a; Gil and Korili, 2016). The policies outside the European Union also tend to manage and recover this waste; thus, recovering of metallic aluminium from aluminium dross (Bruckard and Woodcock, 2007, 2009) or treatment of saline slags by aqueous leaching and Bayer–type digestion (Davies et al., 2008) have been proposed. One of the most attractive recovering method is the use of the saline slag as a precursor of value–added aluminium–containing materials, but for this application a previous treatment of the slag with acid or basic solutions is required to extract the aluminium (Gil et al., 2018b; Yoldi et al., 2019; Santamaría et al., 2020a, 2020b). Jiménez et al. (2021) have very recently reported the preparation of analcime and pollucite zeolites by extraction of Al^{3+} using NaOH or CsOH, respectively, from the same slag used in the present work.

---

* Corresponding author.
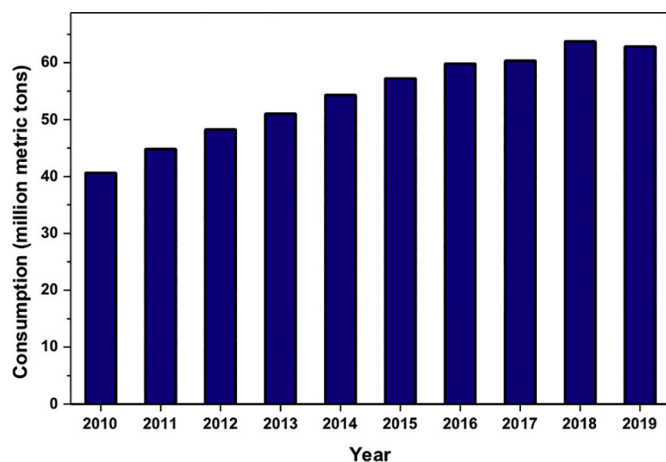 *E-mail address:* vrives@usal.es (V. Rives).

Fig. 1. Consumption of refined aluminium in recent years (World Bureau of Metal Statistics, 2020).

One of the families of materials that can be obtained applying this methodology is that of Layered Double Hydroxides (LDH). They are anionic clays with a general formula $[M(II)_{1-x}M(III)_x(OH)_2]^{x+}[A_{x/n}]^{n-}\cdot mH_2O$, where M(II) and M(III) are divalent and trivalent cations and A is the interlayer anion (Rives, 2001). The structure of LDH is derived from that of brucite, $Mg(OH)_2$; the partial, isomorphical substitution of M(II) by M(III) introduces an excess of positive charge in the $[M(II)_{1-x}M(III)_x(OH)_2]^{x+}$ layer which is balanced by interlayer anions (A^{n-}). When Mg(II) and Al(III) are the cations and carbonate the anion, the compound is known as hydrotalcite. This is a mineral existing in Nature, and probably the most representative of the group (Drits and Bookin, 2001); thus, the solids with its structure are also known as hydrotalcite–like compounds, or simply hydrotalcites. Many divalent cations such as those of Ni, Co, Cu, Mg, Ca or Zn form LDH with trivalent cations such as those of Al, Fe, Cr, Y or Ga (Rives, 2001), while Li as monovalent cation can also form LDH (Serna et al., 1982).

In the same way, many anions such as Cl^-, NO_3^- or CO_3^{2-} can be incorporated into the interlayer region, their interactions being mediated by coulombic forces between the positive charge of the layers and the anions and hydrogen bonding between the hydroxyl groups and the water molecules in the interlayer region (Rives, 2001). Polyoxometalates and anionic coordination compounds have been also incorporated in the interlayer space of these solids (Rives and Ulibarri, 1999). When the divalent cation is Ca^{2+}, the trivalent cation is Al^{3+}, and the anion is chloride, hydroxide or carbonate, the LDH is called hydrocalumite (general formula $Ca_2Al(OH)_6(Cl,CO_3,OH)\cdot H_2O$, for the chloride phase $Ca_2Al(OH)_6Cl\cdot H_2O$) (Hudson Institute of Mineralogy, 2021; Mineralogy Database, 2021). Hydrocalumite (HC), as hydrotalcites, has a wide variety of applications: adsorbent (Takaki et al., 2016), ion–exchanger (Radha et al., 2005; Murayama et al., 2012), antacid (Linares et al., 2016), basic heterogeneous catalysts (Cavani et al., 1991; López-Salinas et al., 1996; Sánchez-Cantú et al., 2015; Granados-Reyes et al., 2017, 2019; Rosset and Perez-Lopez, 2019; Souza Júnior et al., 2020; Szabados et al., 2020) and polymer aditive (Labuschagne et al., 2015; Labuschagné et al., 2019; Zhang et al., 2017).

LDH can be obtained by several methods from their constituting cations, and after its precipitation, the ageing process is very important as it conditions the LDH characteristics, by controlling the phase composition, the particle size, the specific surface area, etc. Ageing can be carried out under reflux, hydrothermal or microwaves conditions. Nowadays, the use of microwaves has increased as it allows to reduce the ageing time and the final solids have similar properties to those aged under traditional methods (Benito et al., 2004, 2008, 2009; Pérez-Barrado et al., 2013; Granados-Reyes et al., 2014; Linares et al., 2016).

The aim of this work is to study the effect of microwave treatment on the formation of several phases in the synthesis of hydrocalumite, using a saline slag as the source of aluminium. Raw saline slag is made up of aggregates of different sizes, containing various aluminium species (various Al_2O_3 phases, $Al(OH)_3$, metallic Al, etc.). Aluminium was recovered from the non–metallic fraction of the saline slag under reflux conditions in a NaOH solution and the resulting liquor was used as a source of aluminium in the synthesis of hydrocalumite. Thus, formation of hydrocalumite is applied itself as a method for recovering of aluminium, forming an Al–based derived solid with added value. This strategy is in line with the circular economy paradigm, in which a waste to be discarded, being itself an environmental problem, receives an added value, changing from an end–of–live situation to an upcycling situation.

2. Experimental procedure

2.1. Materials

Aluminium saline slag was kindly supplied by IDALSA (Ibérica de Aleaciones Ligeras S.L., Spain). The saline slag was ground in a ball mill, using an alumina jar and alumina balls, and then it was sieved with a 1 mm screen. The fraction smaller than 1 mm was washed with water several times until chloride test was negative, and then dried in an oven at 70 °C overnight (Bruckard and Woodcock, 2009; Gil and Korili, 2010, 2016). After the washing treatment, the chloride–free saline slag was sieved with a 0.4 mm light screen, and this fraction, named *small fraction*, was used for the NaOH extraction of aluminium.

The reagents used in this work were HCl (pharma grade, 37%), NaOH (technical grade), $CaCl_2$ (anhydrous, 95%), NaCl (pharma grade), all from Panreac (Spain), being used as received, without any further purification. N_2 (Air Liquide, Spain, 99.999%) was used as an inert, CO_2–free atmosphere.

2.2. Synthesis of hydrocalumite

A portion of 75 g of the small fraction was treated with 250 mL of a 3 M aqueous NaOH solution for 2 h under reflux at 90 °C, while being magnetically stirred. The slurry was separated by filtration. The pH of the liquid was lowered with 2 M aqueous solution of HCl to pH = 1 and it was kept under magnetically stirring for 2 h to precipitate silicon as SiO_2. Then, the white precipitate was separated by filtration. The final acidic aluminium–containing solution was analysed by ICP–OES in order to determine the amount of aluminium extracted.

Hydrocalumite was synthesized by the co–precipitation method (De Roy et al., 2001). A stoichiometric amount of $CaCl_2$ for a Ca/Al molar ratio of 2 (considering the amount of Al determined in the previous step) was dissolved in the acidic aluminium solution and the resulting solution (Ca—Al solution) was bubbled with N_2 in order to avoid the presence of CO_2. A NaOH 2 M aqueous solution, prepared from CO_2–free water, was used to fix the pH at a value of 11.5, using a pH–burette (Crison pH–burette 24). Finally, 15.7 g of NaCl were dissolved in 1 L of CO_2–free water in a 3 L 3–neck round–bottom flask. N_2 was also bubbled through the solution during the synthesis in order to avoid the presence of CO_2 in the reaction medium and the synthesis temperature was 60 °C (Gevers and Labuschagné, 2019). The Ca—Al solution was added with a peristaltic pump (Eldex Laboratories, model PN: 5976 Optos 2SM) at a speed of 5 mL/min over the NaOH solution. After complete addition, the mixture was submitted to microwave treatment (Milestone Ethos Plus Microwave) at temperatures of between 90 and 130 °C for 2 h. Finally, the solids were recovered and washed with CO_2–free water by successive centrifugation steps until the pH of supernatant water was 7 and the solid was then dried at 80 °C in an oven at open air overnight.

The sample obtained without microwave treatment was denoted as *ST*, while the samples obtained after microwave treatment were denoted as *MW–T*, T being the temperature in Celsius; for instance, MW-125 stands for a sample treated with microwave irradiation at 125 °C.

2.3. Characterization techniques

The powder X-ray diffraction (PXRD) patterns were recorded in a Siemens D–5000 instrument using Cu–Kα radiation ($\lambda = 0.154$ nm) with fixed divergence, from 10° to 80° (2θ) at a scanning rate of 2° (2θ)/min with steps of 0.05° and time per step of 1.5 s.

The scanning electron microscopy (SEM) analyses were carried out in a Zeiss EVO HD 25 Scanning Electron Microscope, while the Transmission Electron Microscopy (TEM) analyses were performed using a Tecnai Spirit Twin in 120 kV Transmission Electron Microscope, both at the Nucleus Research Platform, University of Salamanca, Spain.

The FT–IR spectra were recorded in a Perkin–Elmer Spectrum Two instrument with a nominal resolution of 4 cm^{-1} from 4000 to 400 cm^{-1}, using KBr (Merck, grade IR spectroscopy) pressed pellets and averaging 20 scans to improve the signal–to–noise ratio.

Element chemical analyses for several elements were carried out by ICP–OES in a Yobin Ivon Ultima II apparatus (Nucleus Research Platform, University of Salamanca, Spain).

Thermal analyses were performed on a SDT Q600 apparatus (TA Instruments) under a flow of 50 mL/min of oxygen (Air Liquide, Spain, 99.999%) and a temperature heating rate of 10 °C /min from room temperature to 900 °C.

N$_2$–adsorption–desorption isotherms were recorded at −196 °C using a Micromeritics Gemini VII 2390 T. Prior to analysis, N$_2$ was flowed through the sample (ca 0.1 g) at 110 °C for 2 h to remove weakly adsorbed species. Specific surface areas were calculated by the BET method and average pore diameter by the BJH method (Thommes et al., 2015).

3. Results and discussion

3.1. Extraction of aluminium

The aluminium content in the final acid aluminium–containing solution was 7260 mg/L, while other elements were not found. The extraction was carried out under reflux conditions with 3 M NaOH, optimal conditions according with our recent study (Jiménez et al., 2021). The extracted solution was acidified with HCl up to pH = 1, removing by filtration the silica thus precipitated, in order to avoid the formation of silicate-containing compounds.

3.2. Characterization of the solids

The PXRD patterns of the solids are shown in Fig. 2. Calcite, CaCO$_3$ (ICDD 01–072–1937), katoite, Ca$_3$Al$_2$(OH)$_{12}$ (ICDD 01–073–6829) and hydrocalumite (ICDD 01–072–4773) were detected in the solids, which agreed with the phases reported in previous works on the synthesis of this compound (López-Salinas et al., 1996; Radha et al., 2005; Murayama et al., 2012; Pérez-Barrado et al., 2013; Granados-Reyes et al., 2014; Galindo et al., 2014, 2015; Linares et al., 2016). The relative concentrations of these phases depended on the ageing temperature under microwave treatment. Hydrocalumite was detected in all samples, while calcite, clearly identified by its peak at 29°, was only detected in samples ST and MW–90, and its formation may be due to exposure to atmospheric CO$_2$ during sample handling. Although the synthesis was carried out under N$_2$, the reaction mixture was exposed to the atmosphere during handling mainly in the last centrifugation step, and the most alkaline solids may fix enough CO$_2$ to form detectable amounts of calcite. Katoite was clearly detected in samples MW–100 and MW–110, and with very low intensity in MW–120. Hydrocalumite was the only phase detected in samples MW–125 and MW–130. The main difference between both samples was the crystallinity, this being higher for sample MW–125. Hydrocalumite and calcite were formed in the sample not submitted to MW treatment.

Microwave–assisted ageing of the solids allows to obtain highly crystalline materials, decreasing the time of treatment compared to
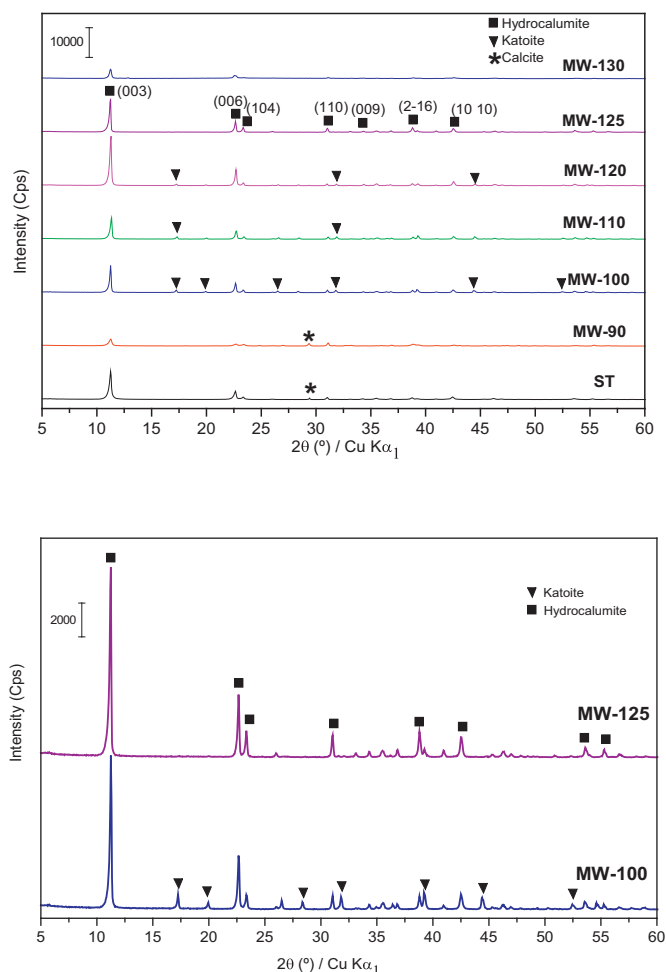

Fig. 2. X-ray patterns of the prepared solids.

conventional ageing in an autoclave or under reflux conditions (Benito et al., 2004, 2008, 2009). Pérez-Barrado et al. (2013) used high temperature (180 °C) for preparing hydrocalumite, detecting calcite in some of the final solids. The structure of their solids was indexed in the trigonal lattice system and belonged to R3c group (No. 161). Granados-Reyes et al. (2014) reported that the interlayer anion can change the crystalline system, chloride leading to a rhombohedral crystal and nitrate leading to a hexagonal crystal. LDH can occur in two classes of polytypes, rhombohedral and hexagonal, with the Al(OH)$_3$ polymorph determining one or the other packing (Williams and O'Hare, 2005). In this work, we used a lower temperature (125 °C) than these authors for preparing pure hydrocalumite and the structure was similar to that indexed in the hexagonal lattice system, group R–3 (No. 148).

As indicated above, hydrocalumite is a layered compound with formula Ca$_2$Al(OH)$_6$Cl·2H$_2$O, where the sheets are built of [Ca$_2$Al(OH)$_6$]$^+$ octahedra, and its structure is similar to that of hydrotalcite (Mg$_6$Al$_2$(OH)$_6$CO$_3$·4H$_2$O), except that Ca and Al octahedra are orderly accommodated in the layers while in hydrotalcites the sheets contain randomly arranged metal hydroxide components (López-Salinas et al., 1996; Souza Júnior et al., 2020). This greater order in the sheets implies more intense and narrower diffraction peaks than in hydrotalcites, but peaks due to (003), (006), (110) and (009) planes are present both in hydrocalumite and hydrotalcite PXRD patterns (Radha et al., 2005). The samples presented a strong preferential orientation, with stacking along crystallographic *c* direction, as shown by the high intensity of the (003) and (006) peaks.

Additionally to hydrocalumite and calcite phases, katoite (ICDD 01–073–6829) was identified in samples MW–100, MW–110 and

MW–120. Katoite is a non–layered double hydroxide with a Ca/Al molar ratio of 1.5 and formula $Ca_3Al_2(OH)_{12}$ (Granados-Reyes et al., 2014). In fact, this is the end–member of a series with formula $Ca_3Al_2(SiO_4)_{3-x}(OH)_{4x}$, that is, when the replacement of SiO_4 by OH is complete (x = 3) (Hudson Institute of Mineralogy, 2021; Mineralogy Database, 2021). To avoid its formation, mainly of the non–end members of the series, it is then desirable to completely remove Si–containing species from the precursor solution. For this reason, as silica can be dissolved as silicate during extraction with NaOH solution, it was removed by lowering the pH to 1, and filtering the SiO_2 thus formed.

The presence of katoite has been reported when the ageing of solids is carried out under microwave irradiation, but it is absent when the ageing is carried out in a conventional autoclave, and long ageing times favour its occurrence (Granados-Reyes et al., 2014). The effect of temperature on the simultaneous formation of katoite and hydrocalumite, has been studied using the respective hydroxides as Ca and Al sources and without applying any ageing treatment, concluding that the use of temperatures above 80–90 °C favoured the appearance of katoite, which competed with hydrocalumite, and suggesting that at a 120 °C only katoite should be present (Gevers and Labuschagné, 2019, 2020). In our solids, a hydrocalumite–katoite mixture existed when the microwave ageing treatment was carried out at temperatures between 100 °C and 120 °C. This suggested that microwave treatment has a positive effect on the kinetics of katoite formation in the temperature range from 100 to 120 °C (Granados-Reyes et al., 2014). In contrast, pure hydrocalumite was obtained at 125 °C and 130 °C.

The theoretical *a* and *c* parameter values for hydrocalumite are 5.75 Å and 23.49 Å, respectively (ICDD 01–072–4773). These cell parameters were calculated for the synthesized solids from the interplanar distances (110), and (003) and (006) ($a = 2d_{(110)}$ and $c = 3/2[d_{(003)} + 2d_{(006)}]$) (Cavani et al., 1991) respectively (Table 1). Cell parameter *a* varied between 5.75 and 5.77 Å; that is, showing values very close to the theoretical one. Similarly, the *c* value varied between 23.51 and 23.63 Å, being very similar, although very slightly higher than the theoretical value. This parameter mainly depends on the charge, size and orientation of the anion between the layers, as well as on the hydration degree (Rousselot et al., 2002; Pérez-Barrado et al., 2013); in the present case the anion was always chloride, although traces of carbonate could be present in some samples. Thus, it is more probable that the small differences found were due to differences in the hydration degree.

Table 1 also shows the crystallite size of the samples along the stacking direction ($d_{(003)}$) and direction (110) ($d_{(110)}$). The crystallite size was calculated from Scherrer's Equation ($D = \frac{k\lambda}{\beta Cos\theta}$; k = 0.94; λ = 0.154 nm; θ = Bragg diffraction angle; $\beta = \sqrt{B^2 - b^2}$; B = FWHM$_{(hkl)}$ (rad); b = instrument width (rad)) (Jenkins and de Vries, 1978). The crystallite size along the stacking direction increased as the treatment temperature increased reaching a maximum for MW–120, and decreasing for higher temperatures. A similar effect was observed for the crystallite size along the (110) direction. The presence of significant amounts of katoite in samples MW–100, MW–110 and MW–120 seemed not to affect the growing of hydrocalumite crystallites. The highest value of the crystallite size along the stacking direction was found for sample MW–125, while the highest value of crystal size in the (110) direction

was observed for sample MW–120. However, when the treatment temperature was 130 °C, a decrease in the crystallite size was observed. Therefore, the MW treatment at 125 °C allowed to obtain pure hydrocalumite with higher crystallinity than at other temperatures.

In those samples where only the hydrocalumite phase was formed (MW–125 and MW–130) the Ca/Al molar ratio was very close to the theoretical value of 2 (Table 1). On the other hand, when hydrocalumite coexisted with katoite, the Ca/Al molar ratio decreased, moving away from the theoretical value of 2 for hydrocalumite, and approaching to the theoretical value of 1.5 for katoite, showing values between 1.79 and 1.88 (as katoite contains less Ca than hydrocalumite, and consequently less Ca than the amount present in the mixture, its excess should remain soluble). Assuming that hydrocalumite and katoite were the two only phases present in the solids, their composition was estimated (Ca/Al = 2 should correspond to pure hydrocalumite and Ca/Al = 1.5 should correspond to pure katoite, intermediate values allowed to estimate the phase composition), katoite being 24–42% of the total amount of these solids. In the case of the solids in which PXRD showed the presence of calcite, the Ca/Al molar ratio was 2.04 (ST) and 1.99 (MW–90). The first of these samples showed a small excess of Ca, but the second one did not show such an excess. The small excess (2%) of found might be forming undetected extraframework phases.

The FT–IR spectra of the solids are shown in Fig. 3. There are few differences between the spectra. In all cases, bands at 3600–3500 cm^{-1} corresponded to stretching vibration of O—H bonds. The band at 3643 cm^{-1} was assigned to stretching vibrations of AlO—H bonds, while the band at 3478 cm^{-1} was assigned to stretching vibrations of CaO—H bonds, and to hydroxyls from water molecules in the interlayer region (Nyquist and Kagel, 2001; Bastida et al., 2004; Albuquerque et al., 2008; Nakamoto, 2008). The presence of water was confirmed by the band at 1618 cm^{-1}, due to its bending mode. The band at 1410 cm^{-1} corresponded to O—CO vibrations of carbonate ions. Its presence indicated that the carbonation of the samples could have occurred during their manipulation, despite the cautions taken to avoid it. This could be in
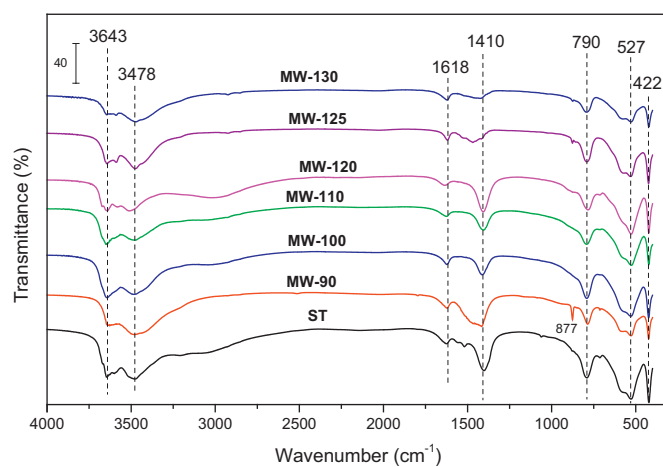

Fig. 3. FT–IR spectra of the samples.

Table 1
Parameters determined for the synthesized solids.

Sample	a (Å)	c (Å)	Ca/Al molar ratio	D$_{(003)}$ (nm)	D$_{(110)}$ (nm)	S$_{BET}$ (m^2/g)	Average Pore diameter (nm)	Phase composition	Hydration water (%)**
ST	5.77	23.63	2.04	45	85	11	7.0	HC + C	15.38
MW–90	5.75	23.59	1.99	29	65	18	6.3	HC + C	14.89
MW–100	5.76	23.61	1.79	74	100	4	6.2	HC + K	9.86
MW–110	5.75	23.51	1.79	60	102	2	5.9	HC + K	8.47
MW–120	5.77	23.57	1.88	62	241	5	5.9	HC + K	13.26
MW–125	5.76	23.63	1.96	87	189	6	6.5	HC	12.31
MW–130	5.75	23.60	1.97	49	110	16	6.1	HC + A*	13.15

HC: Hydrocalumite; K: Katoite; C: Calcite; A: Aragonite (* Traces). ** End of the first mass loss (~ 200 °C).

agreement with the differences found in the values of the cell parameter *c* because the CO_3^{2-} diameter (3.78 Å) (Lide, 1995) is somewhat larger than the Cl^- diameter (3.36 Å) (Lide, 1995). In this way, the presence of carbonate would lead to slightly larger *c* values. The variation of this band was striking, as its intensity decreases with the increase of the treatment temperature. In the spectra of samples MW–125 and MW–130, the band at 1410 cm^{-1} was very weak, so the amount of carbonate must be very small. In fact, PXRD patterns did not show the presence of calcite, so carbonate may be located in the interlayer space, adsorbed on the surface or even forming very small particles of calcite, not detectable by powder X-ray diffraction.

The bands at 790 cm^{-1}, 527 cm^{-1} and 422 cm^{-1} were assigned to M—O bonds, where M was Ca^{2+} or Al^{3+} (Nyquist and Kagel, 2001; Bastida et al., 2004; Albuquerque et al., 2008; Nakamoto, 2008). The weak peak at 877 cm^{-1} for sample MW–90, a mere shoulder for sample ST, is usually assigned to the presence of carbonate (interlayer, contaminant or forming calcite) (Gevers and Labuschagné, 2020; Pan et al., 2020). The same origin can be ascribed for the also weak band/ shoulder close to 1500 cm^{-1}.

The TG and DTG curves of the solids are shown in Fig. 4. The analyses were carried out in air. The thermograms were mostly influenced by the presence of hydrocalumite and katoite. For samples ST and MW–90, containing hydrocalumite and calcite, four mass loss steps can be observed, amounting a total mass loss was close to 40% (Domínguez et al., 2011). The first step, at temperature below 100 °C, was associated to the removal of physisorbed water (López-Salinas et al., 1996; Domínguez et al., 2011). The second step, located close to 140–150 °C, was due to the loss of water in the interlayer space or chemically bound to the LDH (Murayama et al., 2012; Pérez-Barrado et al., 2013; Granados-Reyes et al., 2014). The third step, which appeared close to 300 °C, corresponded to the dehydroxylation of the Ca—Al hydroxide layer. Finally, the fourth step, located around and above 700 °C, could be mainly due to decarbonation of the samples. However, Domínguez et al. (2011) have proposed that the loss of mass around 700 °C could be due to the partial elimination of chlorine–containing species, suggesting that this removal is completed in the form of HCl above 1000 °C.

For samples MW–100, MW–110 and MW–120, in which katoite was identified, the profile of the curves is very similar. The total mass loss was around 30–35%, that is, lower than in previous solids, which agrees with the fact that the reported mass loss for katoite is lower. A significant difference was that the first effect was weaker for samples containing katoite than for only–hydrocalumite samples, indicating a lower amount of adsorbed and crystallization water. In fact, katoite does not contain crystallization water, but only hydroxyl groups (it is also named tricalcium aluminate hexahydrate), and its progressive thermal dehydration is expected to lead tricalcium aluminate, losing six water molecules ($Ca_3Al_2(OH)_{12} \rightarrow Ca_3Al_2O_6 + 6\ H_2O$; 28.6% theoretical mass loss). Thus, the mass loss in these solids was intermediate between that observed for samples in which only hydrocalumite was detected and the mass loss expected for pure katoite.

Samples MW–125 and MW–130, in which the only crystalline phase detected was hydrocalumite, showed thermograms with two loss steps, corresponding to the loss of the hydration water or interlayer water and the dehydroxylation of the Ca—Al LDH. In addition, a very small mass loss was observed at 700 °C. This loss was much smaller than in the previous samples, indicating that the amount of carbonate was very small. This was in agreement with the FT–IR and PXRD results. When the crystallinity of the samples was high, especially in sample MW–125, the dehydration and dehydroxylation temperatures were shifted towards slightly higher values. Higher ordering both in the stacking direction and within the layers implied stronger interactions and, consequently, higher temperatures should be necessary to carry out the processes (Granados-Reyes et al., 2014).

Fig. 5 shows SEM micrographs of some of the solids (see also Fig. S1, Supplementary Material). All samples showed aggregates of hexagonal shaped particles, corresponding to hydrocalumite–type compounds.

However, there were important differences depending on the phases existing in each sample. For sample ST, in which hydrocalumite and calcite were identified by PXRD, only aggregated particles were observed. Nevertheless, for sample MW–90, in which the hydrocalumite and calcite phases were also present, aggregates of particles with an essentially hexagonal shape but with a flaky appearance were observed, as well as needle–shaped particles that could belong to aragonite (Ševčík et al., 2018).

In those samples where hydrocalumite and katoite phases coexisted (MW–100, MW–110 and MW–120), both phases were observed in the SEM micrographs: on one hand, aggregates of hexagonal particles corresponded to LDH–type compounds, and on the other hand, cubic particles corresponded to calcite. Moreover, for the MW–120 sample, perfectly defined and regular octahedra were observed, that may correspond to katoite. Finally, in samples MW–125 and MW–130, only aggregates of hexagonal–shaped particles corresponding to LDH–type compounds were observed. The octahedral particles may become from the cubic ones, as the interconversion between a cube and an octahedron is not unexpected, as both belong to the same symmetry group, and takes place as the crystals grow. Octahedral particles may also correspond to hydrogarnet (Kyritsis et al., 2009; Sánchez-Cantú et al., 2015), which may be formed in trace amounts, if silica was not completely removed (this phase was never detected by XRD).

All the solids prepared showed nitrogen adsorption isotherms (Fig. S2, Supplementary Material) of type II according to the IUPAC classification (Thommes et al., 2015). In addition, all the isotherms showed a H3 type hysteresis loop according to the IUPAC classification (Thommes et al., 2015), corresponding to plate–like particle aggregates leading to slit–like pores. All the solids showed low BET specific surface area values (Table 1), with a maximum of 18 m^2/g, and average pore width in the range of mesopores. The highest BET specific surface area corresponded to samples MW–90 and MW–130, which were the solids with smaller crystallite size. For both samples crystallization was poorer than for the rest of the solids of the series. The better crystallized solids and those containing significant amounts of katoite showed lower values of specific surface area. The values found were in agreement with those reported in the literature (Pérez-Barrado et al., 2013).

4. Conclusions

Hydrocalumite has been synthesized by the coprecipitation method, using the saline slag generated during the recycling process of this metal as a source of aluminium, from which aluminium was solubilized in a strongly basic medium. Several ageing temperatures have been considered under MW irradiation, studying the phases formed in each treatment, and finding that hydrocalumite was present in all of the solids. However, depending on MW ageing temperatures, hydrocalumite coexisted with calcite (treatment at 90 °C) and katoite (treatments at 100, 110 and 120 °C). The optimum ageing temperature under MW irradiation was 125 °C, as it allowed to obtain pure hydrocalumite, with high crystallinity and composed of LDH–type aggregates of regular hexagonal particles. The high crystallinity of the solids justified their low S_{BET} values, which were similar to the values reported in the literature. Globally, solids with textural properties, comparable to those prepared from pure commercial reagents, can be prepared by using the aluminium slag, which suppose a high added value for this residue.

Formation of the different phases under the conditions used is somehow puzzling in some cases. From the thermodynamic point of view, this may be strongly influenced by small variations in the experimental conditions, which may lead to the formation of the different phases. Actually, the temperature of the treatments was not very different (although the presence of hot spots during microwave treatment can be hardly controlled), while the time of treatment was kept constant. Small variations may also occur in the exposure to the atmosphere during handling of the dispersions, thus somewhat facilitating formation of carbonate-containing species. Although the differences
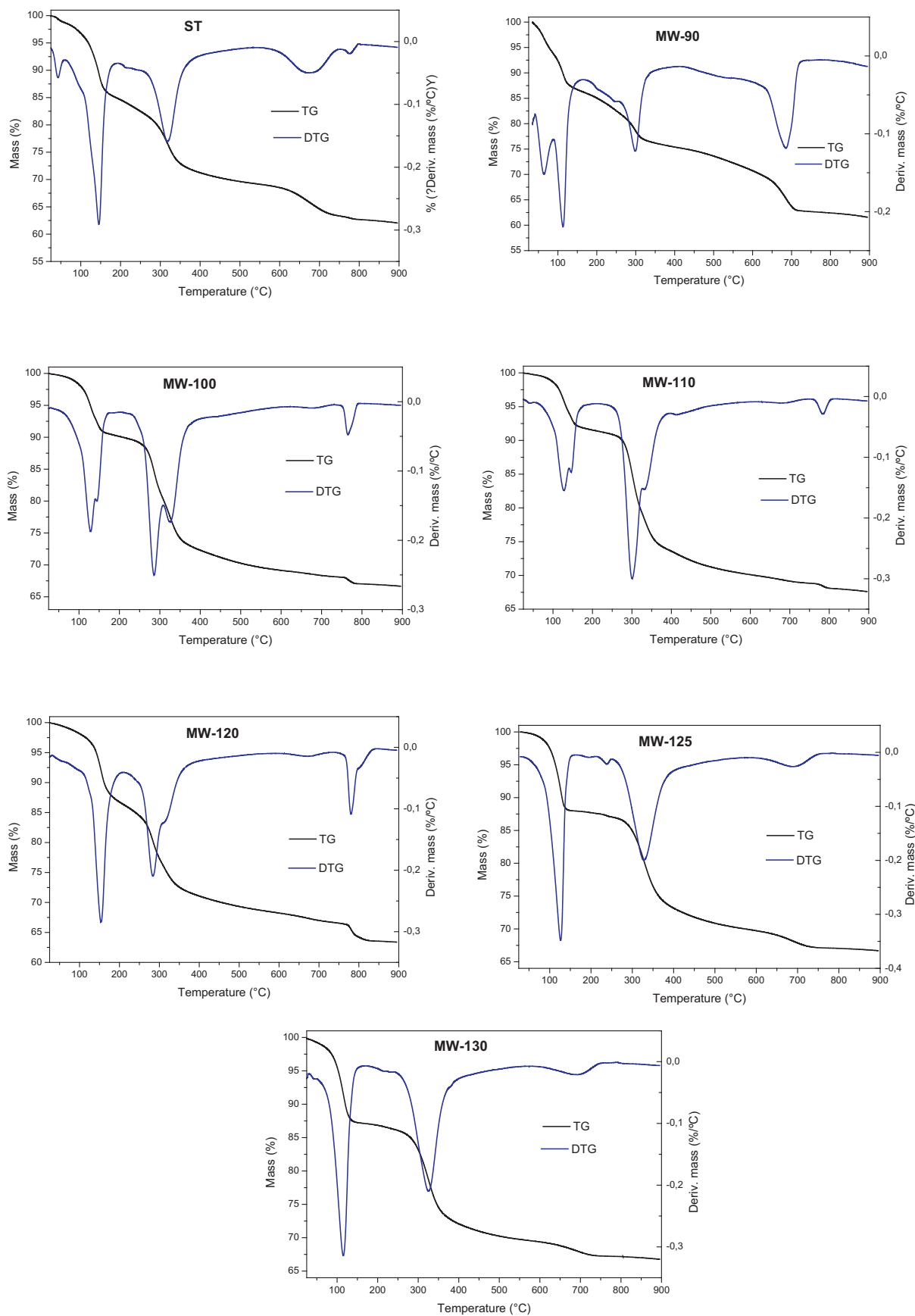
Fig. 4. TG and DTG curves of the prepared solids.
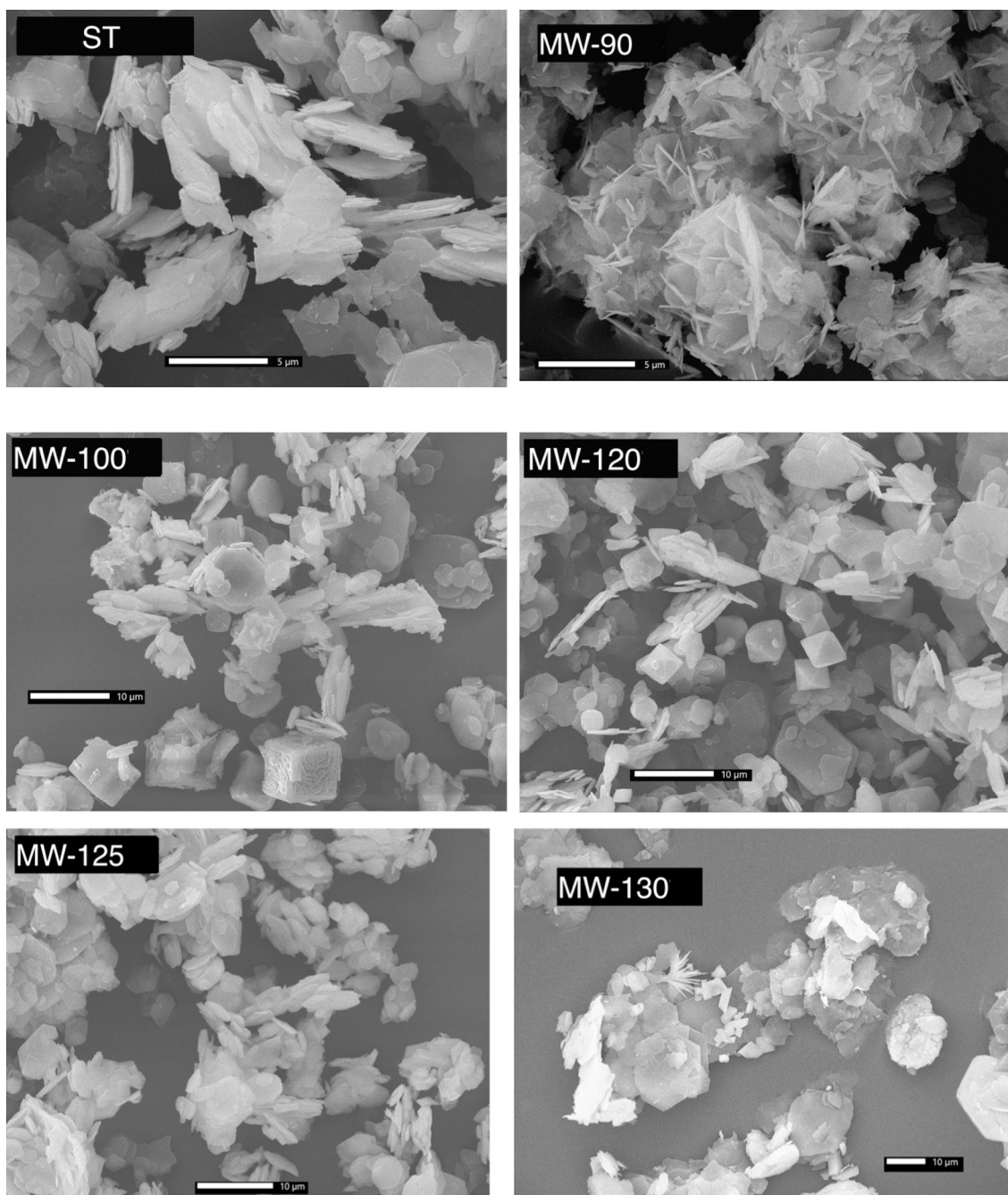
Fig. 5. SEM micrographs of samples.

should be very small, they may condition the formation of the different phases.

Declaration of Competing Interest

The authors declare that they have no known competing financial interests or personal relationships that could have appeared to influence the work reported in this paper.

Acknowledgements

Appendix A. Supplementary data

Supplementary data to this article can be found online at https://doi.org/10.1016/j.clay.2021.106217.

References

Albuquerque, M.C.G., Jiménez-Urbistondo, I., Santamaría-González, J., Mérida-Robles, J.M., Moreno-Tost, R., Rodríguez-Castellón, E., Jiménez-López, A., Azevedo, D.C.S., Cavalcante Jr., C.L., Maireles-Torres, P., 2008. CaO supported on mesoporous silicas as basic catalysts for transesterification reactions. Appl. Catal. A 334, 35–43. https://doi.org/10.1016/j.apcata.2007.09.028.

Bastida, J., Bolós, C., Pardo, P., Serrano, F.J., 2004. Análisis microestructural por DRX de CaO obtenido a partir de carbonato cálcico molido (CCM). Bol. Soc. Esp. Ceram. Vidr. 43, 80–83. https://doi.org/10.3989/cyv.2004.v43.i1.621.

Benito, P., Labajos, F.M., Rives, V., 2004. Incidencia de la radiación microondas en la cristalinidad de materiales laminares. Bol. Soc. Esp. Ceram. Vidr. 43, 56–58. https://doi.org/10.3989/cyv.2004.v43.i1.615.

Benito, P., Guinea, I., Labajos, F.M., Rocha, J., Rives, V., 2008. Microwave-hydrothermally aged Zn, Al hydrotalcite-like compounds: influence of the composition and the irradiation conditions. Micropor. Mesopor. Mater. 110, 292–302. https://doi.org/10.1016/j.micromeso.2007.06.013.

Benito, P., Labajos, F.M., Rives, V., 2009. Microwaves and layered double hydroxides: a smooth understanding. Pure Appl. Chem. 81, 1459–1471. https://doi.org/10.1351/PAC-CON-08-07-01.

Bruckard, W.J., Woodcock, J.T., 2007. Characterisation and treatment of Australian salt cakes by aqueous leaching. Miner. Eng. 20, 1376–1390. https://doi.org/10.1016/j.mineng.2007.08.020.

Bruckard, W.J., Woodcock, J.T., 2009. Recovery of valuable materials from aluminium salt cakes. Int. J. Miner. Process. 93, 1–5. https://doi.org/10.1016/j.minpro.2009.05.002.

Cavani, F., Trifirò, F., Vaccari, A., 1991. Hydrotalcite-type anionic clays: preparation, properties and applications. Catal. Today 11, 173–301. https://doi.org/10.1007/BF03263563.

Davies, M., Smith, P., Bruckard, W.J., Woodcock, J.T., 2008. Treatment of salt cakes by aqueous leaching and Bayer-type digestion. Miner. Eng. 21, 605–612. https://doi.org/10.1016/j.mineng.2007.12.001.

De Roy, A., Forano, C., Besse, J.P., 2001. Layered double hydroxides: synthesis and post-synthesis modification. In: Rives, V. (Ed.), Layered Double Hydroxides, 1. Nova Science Publishers, Inc, New York, pp. 1–39.

Directive 2010/75/EU of the European Parliament and of the Council, 24 November 2010. On Industrial Emissions (Integrated Pollution Prevention and Control). Official Journal of the European Union (17.12.2010, L 334/17).

Domínguez, M., Pérez-Bernal, M.E., Ruano-Casero, R.J., Barriga, C., Rives, V., Ferreira, R.A.S., Carlos, L.D., Rocha, J., 2011. Multiwavelength luminescence in lanthanide-doped hydrocalumite and mayenite. Chem. Mater. 23, 1993–2004. https://doi.org/10.1021/cm200408x.

Drits, V.A., Bookin, A.S., 2001. Crystal structure and X-ray identification of layered double hydroxides. In: Rives, V. (Ed.), Layered Double Hydroxides, 2. Nova Science Publishers, Inc, New York, pp. 41–100.

Galindo, R., López-Delgado, A., Padilla, I., Yates, M., 2014. Hydrotalcite-like compounds: a way to recover a hazardous waste in the aluminium tertiary industry. Appl. Clay Sci. 95, 41–49. https://doi.org/10.1016/j.clay.2014.03.022.

Galindo, R., López-Delgado, A., Padilla, I., Yates, M., 2015. Synthesis and characterisation of hydrotalcites produced by an aluminium hazardous waste: a comparison between the use of ammonia and the use of triethanolamine. Appl. Clay Sci. 115, 115–123. https://doi.org/10.1016/j.clay.2015.07.032.

Gevers, B.R., Labuschagné, F.J.W.J., 2019. Temperature effects on the dissolution-precipitation synthesis of hydrocalumite. AIP Conf. Proc. 2055 https://doi.org/10.1063/1.5084829.

Gevers, B.R., Labuschagné, F.J.W.J., 2020. Green synthesis of hydrocalumite (CaAl-OH-LDH) from Ca(OH)$_2$ and Al(OH)$_3$ and the parameters that influence its formation and speciation. Crystals 10, 1–26. https://doi.org/10.3390/cryst10080672.

Gil, A., 2005. Management of the salt cake from secondary aluminum fusion processes. Ind. Eng. Chem. Res. 44, 8852–8857. https://doi.org/10.1021/ie050835o.

Gil, A., Korili, S.A., 2010. In: Sarkar, S.K. (Ed.), Management of the Salt Cake Generated at Secondary Aluminium Melting Plants, Chapter 7 in Environmental Management. Intechopen. https://doi.org/10.5772/10104.

Gil, A., Korili, S.A., 2016. Management and valorization of aluminum saline slags: current status and future trends. Chem. Eng. J. 289, 74–84. https://doi.org/10.1016/j.cej.2015.12.069.

Gil, A., Albeniz, S., Korili, S.A., 2014. Valorization of the saline slags generated during secondary aluminium melting processes as adsorbents for the removal of heavy metal ions from aqueous solutions. Chem. Eng. J. 251, 43–50. https://doi.org/10.1016/j.cej.2014.04.056.

Gil, A., Arrieta, E., Vicente, M.A., Korili, S.A., 2018a. Application of industrial wastes from chemically treated aluminum saline slags as adsorbents. ACS Omega 3, 18275–18284. https://doi.org/10.1021/acsomega.8b02397.

Gil, A., Arrieta, E., Vicente, M.A., Korili, S.A., 2018b. Synthesis and CO$_2$ adsorption properties of hydrotalcite-like compounds prepared from aluminum saline slag wastes. Chem. Eng. J. 334, 1341–1350. https://doi.org/10.1016/j.cej.2017.11.100.

Granados-Reyes, J., Salagre, P., Cesteros, Y., 2014. Effect of microwaves, ultrasounds and interlayer anion on the hydrocalumites synthesis. Micropor. Mesopor. Mater. 199, 117–124. https://doi.org/10.1016/j.micromeso.2014.08.004.

Granados-Reyes, J., Salagre, P., Cesteros, Y., 2017. Effect of the preparation conditions on the catalytic activity of calcined Ca/Al-layered double hydroxides for the synthesis of glycerol carbonate. Appl. Catal. A Gen. 536, 9–17. https://doi.org/10.1016/j.apcata.2017.02.013.

Granados-Reyes, J., Salagre, P., Cesteros, Y., Busca, G., Finocchio, E., 2019. Assessment through FT-IR of surface acidity and basicity of hydrocalumites by nitrile adsorption. Appl. Clay Sci. 180, 105180. https://doi.org/10.1016/j.clay.2019.105180.

Hudson Institute of Mineralogy, 2021. Hydrocalumite: https://www.mindat.org/min-1968.html; Katoite: https://www.mindat.org/min-2167.html.

Jenkins, R., de Vries, J.L., 1978. Worked Examples in X-ray Analysis, Second Edition (Part of the Philips Technical Library Book Series (PTL)). Springer.

Jiménez, A., Misol, A., Morato, A., Rives, V., Vicente, M.A., Gil, A., 2021. Synthesis of pollucite and analcime zeolites by recovering aluminum from a saline slag. J. Clean. Prod. 297, 126667. https://doi.org/10.1016/j.jclepro.2021.126667.

Kyritsis, K., Meller, N., Hall, C., 2009. Chemistry and morphology of hydrogarnets formed in cement-based CASH hydroceramics cured at 200° to 350°C. J. Am. Ceram. Soc. 92, 1105–1111. https://doi.org/10.1111/j.1551-2916.2009.02958.x.

Labuschagne, F.J.W.J., Molefe, D.M., Focke, W.W., van der Westhuizen, I., Wright, H.C., Royeppen, M.D., 2015. Heat stabilising flexible PVC with layered double hydroxide derivatives. Polym. Degrad. Stabil. 113, 46–54. https://doi.org/10.1016/j.polymdegradstab.2015.01.016.

Labuschagné, J., Molefe, D., Focke, W.W., Ofosu, O., 2019. Layered double hydroxide derivatives as flame retardants for flexible PVC. Macromol. Symp. 384, 1800148. https://doi.org/10.1002/masy.201800148.

Lide, D.R. (Ed.), 1995. CRC Handbook of Chemistry and Physics, 76th edition. CRC Press, Boca Raton, USA.

Linares, C.F., Moscosso, J., Alzurutt, V., Ocanto, F., Bretto, P., González, G., 2016. Carbonated hydrocalumite synthesized by the microwave method as a possible antacid. Mater. Sci. Eng. C 61, 875–878. https://doi.org/10.1016/j.msec.2016.01.007.

López-Salinas, E., Serrano, M.E.L., Jácome, M.A.C., Secora, I.S., 1996. Characterization of synthetic hydrocalumite-type [Ca$_2$Al(OH)$_6$]NO$_3$·mH$_2$O: effect of the calcination temperature. J. Porous. Mater. 2, 291–297. https://doi.org/10.1007/BF00489810.

Mineralogy Database, 2021. Hydrocalumite: http://webmineral.com/data/Hydrocalumite.shtml#.YMeTjfJxeUl; Katoite: http://webmineral.com/data/Katoite.shtml#.YE-CaLCg-Ul.

Murayama, N., Maekawa, I., Ushiro, H., Miyoshi, T., Shibata, J., Valix, M., 2012. Synthesis of various layered double hydroxides using aluminum dross generated in aluminum recycling process. Int. J. Miner. Process. 110–111, 46–52. https://doi.org/10.1016/j.minpro.2012.03.011.

Nakamoto, K., 2008. Infrared and Raman Spectra of Inorganic and Coordination Compounds: Part A: Theory and Applications in Inorganic Chemistry. John Wiley & Sons, Sixth Edition.

Nyquist, R.A., Kagel, R.O., 2001. Infrared Spectra of Inorganic Compounds. Academic Press, New York.

Pan, X., Liu, J., Wu, S., Yu, H., 2020. Formation behavior of tricalcium aluminate hexahydrate in synthetic sodium aluminate solution with high alkali concentration and caustic ratio. Hydrometallurgy 195, 105373. https://doi.org/10.1016/j.hydromet.2020.105373.

Pérez-Barrado, E., Pujol, M.C., Aguiló, M., Cesteros, Y., Díaz, F., Pallarès, J., Marsal, L.F., Salagre, P., 2013. Fast aging treatment for the synthesis of hydrocalumites using microwaves. Appl. Clay Sci. 80–81, 313–319. https://doi.org/10.1016/j.clay.2013.05.006.

Radha, A.V., Kamath, P.V., Shivakumara, C., 2005. Mechanism of the anion exchange reactions of the layered double hydroxides (LDHs) of Ca and Mg with Al. Solid State Sci. 7, 1180–1187. https://doi.org/10.1016/j.solidstatesciences.2005.05.004.

Rives, V. (Ed.), 2001. Layered Double Hydroxides. Nova Science Publishers, Inc., New York.

Rives, V., Ulibarri, M.A., 1999. Layered double hydroxides (LDH) intercalated with metal coordination compounds and oxometalates. Coord. Chem. Rev. 181, 61–120. https://doi.org/10.1016/S0010-8545(98)00216-1.

Rosset, M., Perez-Lopez, O.W., 2019. Cu–Ca–Al catalysts derived from hydrocalumite and their application to ethanol dehydrogenation. React. Kinet. Mech. Catal. 126, 497–511. https://doi.org/10.1007/s11144-018-1513-y.

Rousselot, I., Taviot-Guého, C., Leroux, F., Léone, P., Palvadeau, P., Besse, J.P., 2002. Insights on the structural chemistry of hydrocalumite and hydrotalcite-like materials: investigation of the series Ca$_2$M^{3+}(OH)$_6$Cl·2H$_2$O (M^{3+}: Al^{3+}, Ga^{3+}, Fe^{3+}, and Sc^{3+}) by X-ray powder diffraction. J. Solid State Chem. 167, 137–144. https://doi.org/10.1006/jssc.2002.9635.

Sánchez-Cantú, M., Camargo-Martínez, S., Pérez-Díaz, L.M., Hernández-Torres, M.E., Rubio-Rosas, E., Valente, J.S., 2015. Innovative method for hydrocalumite-like compounds' preparation and their evaluation in the transesterification reaction. Appl. Clay Sci. 114, 509–516. https://doi.org/10.1016/j.clay.2015.07.004.

Santamaría, L., López-Aizpún, M., García-Padial, M., Vicente, M.A., Korili, S.A., Gil, A., 2020a. Zn-Ti-Al layered double hydroxides synthesized from aluminum saline slag wastes as efficient drug adsorbents. Appl. Clay Sci. 187, 105486. https://doi.org/10.1016/j.clay.2020.105486.

Santamaría, L., Vicente, M.A., Korili, S.A., Gil, A., 2020b. Saline slag waste as an aluminum source for the synthesis of Zn-Al-Fe-Ti layered double-hydroxides as catalysts for the photodegradation of emerging contaminants. J. Alloys Compd. 843, 156007. https://doi.org/10.1016/j.jallcom.2020.156007.

Serna, C., Rendon, J., Iglesias, J., 1982. Crystal-chemical study of layered (Al$_2$Li(OH)$_6$)$^+$X$^-$.nH$_2$O. Clays Clay Miner. 30, 180–184.

Ševčík, R., Šašek, P., Viani, A., 2018. Physical and nanomechanical properties of the synthetic anhydrous crystalline CaCO$_3$ polymorphs: vaterite, aragonite and calcite. J. Mater. Sci. 53, 4022–4033. https://doi.org/10.1007/s10853-017-1884-x.

Souza Júnior, R.L., Rossi, T.M., Detoni, C., Souza, M.M.V.M., 2020. Glycerol carbonate production from transesterification of glycerol with diethyl carbonate catalyzed by Ca/Al-mixed oxides derived from hydrocalumite. Biomass Convers. Biorefine. https://doi.org/10.1007/s13399-020-01110-4.

Sverdlin, A., 2003. In: Totten, E. (Ed.), Handbook of Aluminum. Marcel Dekker, Inc. https://doi.org/10.1201/9780203912607.

Szabados, M., Adél Ádám, A., Traj, P., Muráth, S., Baán, K., Bélteky, P., Kónya, Z., Kukovecz, Á., Sipos, P., Pálinkó, I., 2020. Mechanochemical and wet chemical syntheses of CaIn-layered double hydroxide and its performance in a transesterification reaction compared to those of other Ca$_2$M(III) hydrocalumites (M: Al, Sc, V, Cr, Fe, Ga) and Mg(II)-, Ni(II)-, Co(II)- or Zn(II)-based hydrotalcites. J. Catal. 391, 282–297. https://doi.org/10.1016/j.jcat.2020.07.038.

Takaki, Y., Qiu, X., Hirajima, T., Sasaki, K., 2016. Removal mechanism of arsenate by bimetallic and trimetallic hydrocalumites depending on arsenate concentration. Appl. Clay Sci. 134, 26–33. https://doi.org/10.1016/j.clay.2016.05.010.

Thommes, M., Kaneko, K., Neimark, A.V., Olivier, J.P., Rodriguez-Reinoso, F., Rouquerol, J., Sing, K.S.W., 2015. Physisorption of gases, with special reference to the evaluation of surface area and pore size distribution (IUPAC Technical Report). Pure Appl. Chem. 87, 1051–1069. https://doi.org/10.1515/pac-2014-1117.

Tsakiridis, P.E., 2012. Aluminium salt slag characterization and utilization - a review. J. Hazard. Mater. 217–218, 1–10. https://doi.org/10.1016/j.jhazmat.2012.03.052.

Tsakiridis, P.E., Oustadakis, P., Agatzini-Leonardou, S., 2013. Aluminium recovery during black dross hydrothermal treatment. J. Environ. Chem. Eng. 1, 23–32. https://doi.org/10.1016/j.jece.2013.03.004.

Williams, G.R., O'Hare, D., 2005. Factors influencing staging during anion-exchange intercalation into $[LiAl_2(OH)_6]X \cdot mH_2O$ ($X = Cl^-$, Br^-, NO_3^-). Chem. Mater. 17, 2632–2640. https://doi.org/10.1021/cm0503275.

World Bureau of Metal Statistics, 2020. http://www.world-bureau.com/.

Yoldi, M.E., Fuentes-Ordoñez, G., Korili, S.A., Gil, A., 2019. Zeolite synthesis from industrial wastes. Microporous Mesoporous Mater. 287, 183–191. https://doi.org/10.1016/j.micromeso.2019.06.009.

Zhang, Q., Jiao, Q., Leroux, F., Tang, P., Li, D., Feng, Y., 2017. Antioxidant intercalated hydrocalumite as multifunction nanofiller for Poly(propylene): synthesis, thermal stability, light stability, and anti-migration property. Polym. Degrad. Stabil. 140, 9–16. https://doi.org/10.1016/j.polymdegradstab.2017.04.012.